Available online at www.sciencedirect.com
ScienceDirect
Cement & Concrete Composites 30 (2008) 255–265
Cement & Concrete Composites
www.elsevier.com/locate/cemconcomp

Long-term aging of fiber-cement corrugated sheets – The effect of carbonation, leaching and acid rain

C.M.R. Dias [a,*], M.A. Cincotto [a], H. Savastano Jr. [b], V.M. John [a,*]

[a] Department of Construction Engineering, Escola Politécnica, University of São Paulo (USP), 05508 900 São Paulo-SP, Brazil
[b] Faculdade de Zootecnia e Engenharia de Alimentos, University of São Paulo (USP), Avenida Duque de Caxias Norte, 225, 13635-900 Pirassununga, São Paulo, Brazil

Received 5 March 2007; received in revised form 1 November 2007; accepted 3 November 2007
Available online 19 November 2007

Abstract

This paper studies the performance of fiber-cement corrugated sheets exposed to long-term weathering, exploring the effect of different environments on fiber-cement degradation. Fiber-cement corrugated sheets that had been exposed to weathering, and in place for more than 30-years, were collected from two different Brazilian cities (São Paulo and Criciúma). Mechanical properties (MOR, MOE and fracture toughness) were tested on samples removed from the corrugated sheets. Microstructure was evaluated by X-ray diffraction, SEM with EDS analysis, MIP and TG. The results show that the 37-year-old asbestos-cement corrugated sheets from São Paulo presented similar characteristics to those of the non-aged asbestos-cement readily available on the market place. Conversely, deterioration of the asbestos-cement from the industrial area of Criciúma is related to acidic attack, along with carbonation and leaching as a consequence of continued exposition to acid rain during several decades. This process resulted in higher porosity and lower mechanical strength, revealing that leaching mechanisms can have important effect on the performance of thin fiber-cement sheets.

Keywords: Fiber reinforcement (E); Mechanical properties (C); Microstructure (B); Aging (C); Characterization (B)

1. Introduction

Asbestos-cement is known to be a very durable material [1], yet little has been published on the theme regarding long-term results. Most of the data published concerning fiber cement durability discusses asbestos-free compositions, where significant attention is given to the deterioration of organic fibers. In contrast, not much attention has been given to the deterioration of the matrix, which proportionally affects the performance of the composite.

The matrix of fiber-cement corrugated sheets can suffer deterioration similar to the matrixes of other Portland cement-based products such as concrete and mortars, from chemically aggressive agents. Additionally, damage can also be generated by mechanical stress due to stockpiling, transportation, assembling activities and in use exposure to wind, moisture, thermal cycles and other climate factors [2].

The cementitious matrix of fiber-cement corrugated sheets can also suffer deterioration through water leaching. Water leaching of Portland cement-based materials has been widely studied and it is well established that this mechanism of deterioration can generate a weakening in composites [3–5]. Compounds, such as portlandite, ettringite, gypsum and C–S–H can be removed from the matrix by percolation or flow of water [3]. The effect of cement matrix leaching by rainwater on mechanical performance is neglected in most situations. However, fiber-cement sheets are very thin (~4–10 mm), and even shallow depths of corrosion can generate significant impact on the bending strength. Asbestos reinforced fiber-cement that have

* Corresponding authors. Tel.: +55 11 30915794; fax: +55 11 30915544 (V.M. John, C.M.R. Dias).
E-mail addresses: cleber.dias@poli.usp.br (C.M.R. Dias), john@poli.usp.br (V.M. John).

0958-9465/$ - see front matter © 2007 Elsevier Ltd. All rights reserved.
doi:10.1016/j.cemconcomp.2007.11.001

undergone the effects of leaching can release asbestos fibers into the environment [6].

Acid rain, resulting from SO_x pollution, can provoke an even more intense deterioration than leaching. Deterioration from sulfate attack has been widely reported in cement-based materials such as concrete and mortar [3,7–11]. As the deterioration starts at the surface, it proceeds inwardly to the material's core where it creates a deteriorated layer [9]. Xie et al. [10] have detailed the mechanism of acid rain attacks in concrete. Zivica and Bajzab [11] used the following simplified equations to explain the acidic attack of cement-based materials:

$$H_2SO_4 + Ca(OH)_2 \rightarrow CaSO_4 \cdot 2H_2O \quad (1)$$

$$3CaSO_4 + 3CaO \cdot Al_2O_3 \cdot 6H_2O + 25H_2O \rightarrow 3CaO \cdot Al_2O_3 \cdot 3CaSO_4 \cdot (31\text{–}32)H_2O \quad (2)$$

Deterioration proceeds with the carbonation of ettringite, which forms more gypsum (a soluble product), calcium carbonate and aluminum hydroxide (insoluble products) and releases water [12,13], as described by the following reaction [14]:

$$C_3A \cdot 3CaSO_4 \cdot 32H_2O + 3CO_2 \rightarrow 3CaCO_3 + 3CaSO_4 \cdot 2H_2O + Al_2O_3 \cdot xH_2O + (26 - x)H_2O \quad (3)$$

This work intends to assess the in-use effects of aging on the properties of asbestos-cement corrugated sheets, collected from two distinct Brazilian urban environments, exploring the influence of the environment on aging process. Knowledge of the mechanisms of deterioration and long-term performance of fiber-cement composites under tropical climate conditions will contribute to the development of non-asbestos technologies in Brazil and other developing countries that are trying to access a substitute for asbestos.

2. Experimental

2.1. Test samples

Samples with geometry presented in Table 1 were extracted from aged asbestos-cement roof sheets produced by Hatschek process, from two building roofs located São Paulo and Criciúma respectively. São Paulo, a large industrial metropolis, has a mean annual temperature of 19.5 °C, an annual rainfall of ~1500 mm, a mean relative humidity of 78% and presents urban and industrial pollution. The samples from São Paulo are corrugated sheets that had been exposed to the elements for 37 years while serving as part of the roof of the School of Communication and Arts (23°33′S, 46°43′W, ~725 m of altitude) at the University of São Paulo (ECA – USP). As imprinted on its internal surface, USP's corrugated sheets comply with the Brazilian Standard EB93 (1957), which among other aspects, did require a minimal flexural load of 5 kN/m. This is the same minimum strength specified by Brazilian Standard NBR 7581 (1993), applied to the new corrugated sheets.

Table 1
Average dimensions with standard deviation of specimens and bending spans

Specimens	Thickness (mm)	Width (mm)	Bending span (mm)
Non-aged	5.5 ± 0.1	30.0 ± 1.3	135
USP	5.7 ± 0.7	32.9 ± 1.0	160
CRI	9.2 ± 0.1	24.2 ± 0.2	180

The samples from Criciúma are from roof sheets designed for large spans, presenting a "W shaped" cross-section. Criciúma, which is located in the state of Santa Catarina in the south of Brazil, concentrates coal-mining activities, coal power stations, and registers intense occurrences of acid rain. The city has a mean annual temperature of ~19 °C, an annual rainfall of 1400 mm and an average relative humidity of 81%. The samples from Criciúma, labeled CRI, were taken from a 30-year-old industrial roof located in an industrial area of the city (28°40′S, 49°20′W, ~60 m of altitude). As a reference, non-aged asbestos-cement corrugated sheets (labeled non-aged) available in the local market, were also evaluated.

2.2. Methods

All tests were conducted on specimens taken from the non-curved regions of the corrugated sheets (Fig. 1). These were extracted using a high-speed, water-cooled rotary saw. Thermogravimetric analyses were conducted with a NETZSCH STA409 PG using a sample mass of approximately 1.0 g and nitrogen atmosphere (flow ratio = 60 mL/min), heating ratio of 10 °C/min up to maximum temperature of 1000 °C. Prior to testing, the samples were dried at 40 °C under low pressure (−60 kPa) for 24 h to remove any moisture.

Insoluble residue was evaluated with an acidic attack (HCl solution 1:50) on ground samples, followed by drying at 100 °C. The results are expressed in percentages of total weight.

Image analysis (Image Pro Plus) of specimens' cross-sections after the application of phenolphthalein solution determined carbonation depth. XRD was performed using a Philips MPD1880, radiation Cuα, 0.02 (2θ) step and 1 s

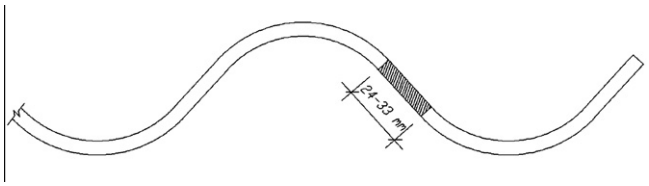

Fig. 1. Schematic cross-section of a corrugated sheet with the indication of the region from where the specimens were extracted for the experimental tests.

counting time. The asbestos-cement samples were submitted to SEM/EDS analysis. A LEO Leika S440 microscope with an acceleration voltage of 20 kV and current of 150 mA was used to examine the fractured section, the polished cross-section and the surface of specimens. Cross-section surfaces of samples for evaluation by backscattering electron image analysis (BSEI) and SEM, were vacuum (200 mbar) impregnated with epoxy resin and air cured for 24 h before grinding with silicon carbide and polishing with diamond paste (3, 1 and 1/4 μm grain sizes respectively). The surfaces of the aged samples were gently washed with water prior to SEM examination in order to remove the superficial patina crust, exposing the cementitious surface. All samples received carbon coating before SEM examination.

MIP tests were carried out using a Micromeritics Auto Pore III and previously dried samples (70 ± 5 °C at −60 kPa). The Washburn equation with a contact angle of 130° and mercury superficial tension of 485×10^{-3} N/m determined the pore size distribution [15]. Two 1 g specimens from each series were submitted to evaluation.

Four-point bending tests (15 specimens/sample) were conducted with an INSTRON 5569 using different size specimens and bending spans (Table 1). Displacement rate was controlled (1.5 mm/min) and deflection measured with a LVDT positioned under the specimens in the middle of the span. Modulus of rupture (MOR), modulus of elasticity (MOE) and fracture toughness of specimens were evaluated. Fracture toughness of fiber reinforced materials "can be considered as their energy absorption capacity which is conventionally characterized by the area under the load–displacement curve obtained experimentally" [16]. All specimens were soaked in water for 24 h before bending tests.

3. Results and discussion

3.1. Carbonation depth

Fig. 2 presents the cross-section images of specimens after the application of the phenolphthalein solution. Dark regions in the cross-sections represent non-carbonated areas. The images show that non-aged specimens suffered diffuse carbonation in the peripheral region (Fig. 2a), which probably occurred during exposure in the laboratory environment. The USP specimens were totally carbonated (Fig. 2b). CRI specimens present superficially carbonated layers (Fig. 2c). In this case, carbonation depth is non-uniform, being deeper in the outer layer not exposed to rain. The average depth is 3.3 mm, which is equivalent to 36% of the total cross-section area of the specimens. The outer layers (CRI-deteriorated layers) had a visually distinct appearance, resembling the effects of deterioration. Surprisingly however, little or no carbonation was observed in the core of the CRI samples, despite being in service for about the same amount of time as those from USP.

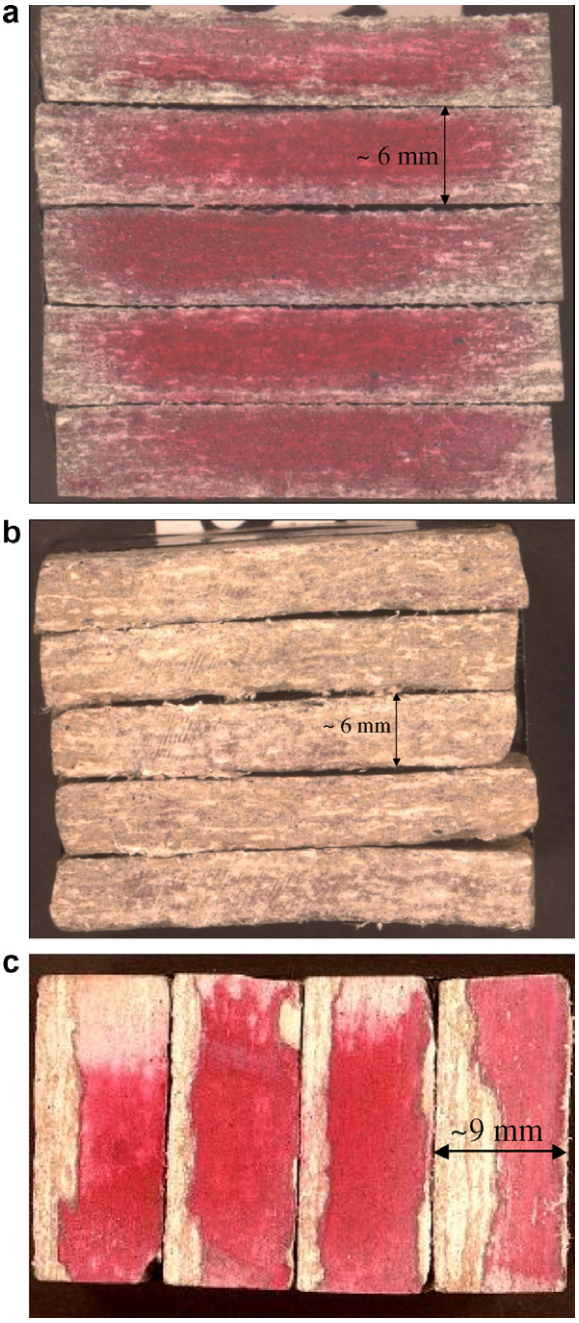

Fig. 2. Carbonation depth: (a) non-aged, (b) USP and (c) CRI specimens.

3.2. Chemical and mineralogical composition

Fig. 3 presents X-ray diffraction patterns of the samples. Calcite, chrysotile peaks and vaterite vestiges were identified in all samples. Diffuse peaks at 18.7 nm (48.6°), 19.1 nm (47.6°) and 19.3 nm (47.3°) of non-aged samples, similarly to those reported by Cole and Kroone [17], confirmed the presence of poorly crystallized calcite. Anhydrous calcium silicate (alite and belite) peaks and dolomite peaks were only found in the non-aged asbestos-cement, showing that the matrix of this sample had not yet completely hydrated and confirming a recent

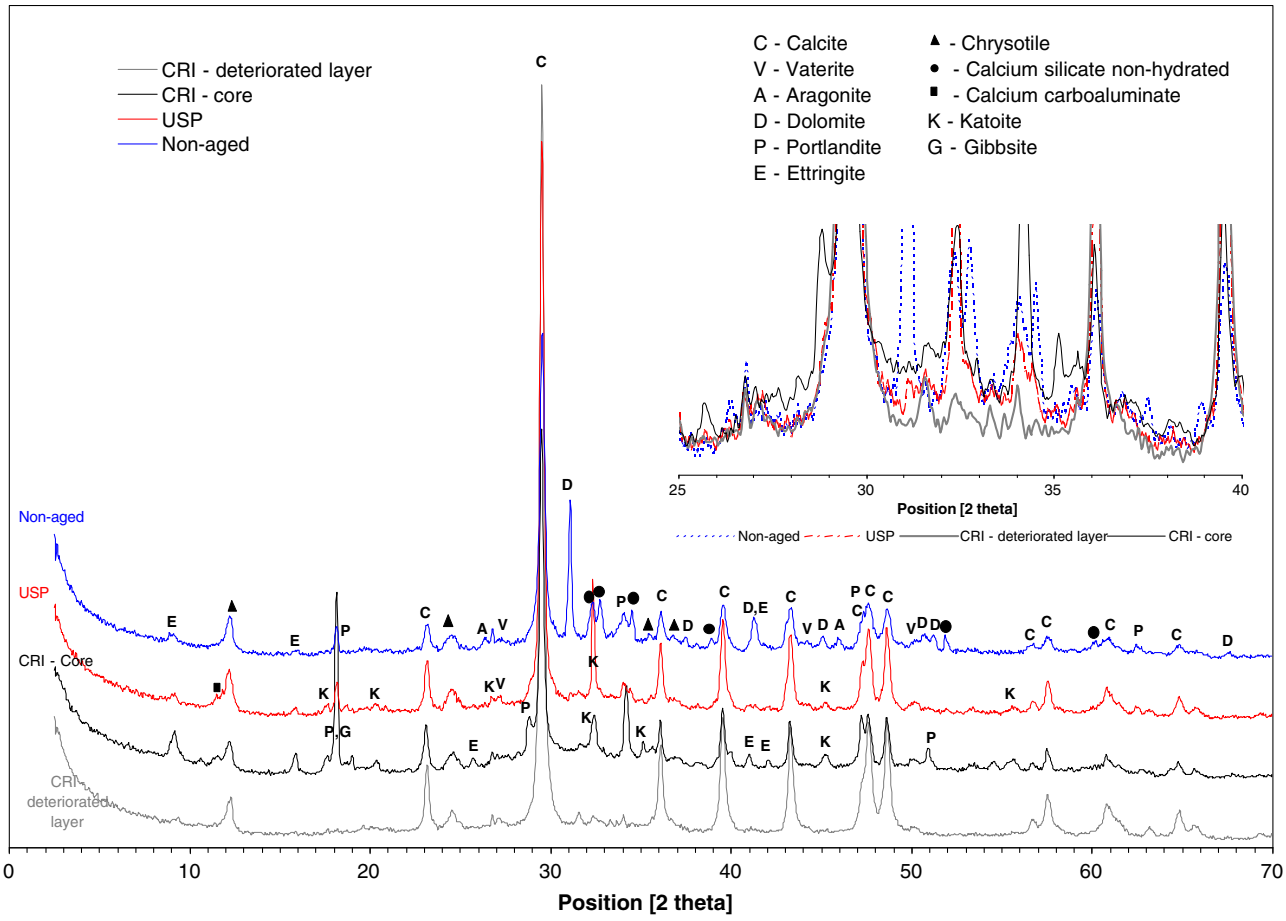

Fig. 3. X-ray diffraction patterns of samples with details at $25° < 2\theta < 40°$.

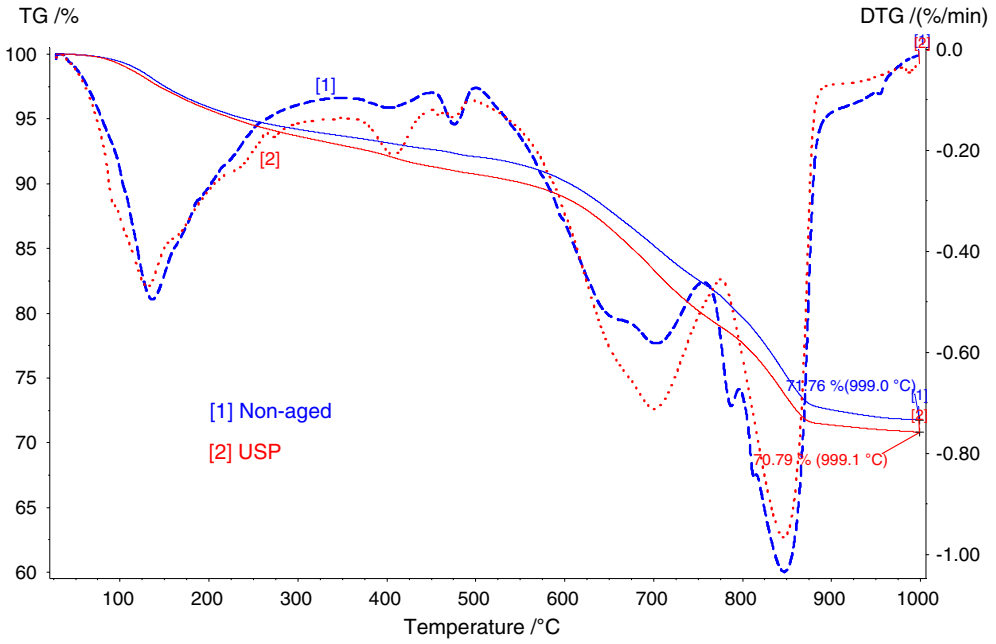

Fig. 4. TG and DTG curves of non-aged and USP specimens.

Brazilian market trend of using dolomite as filler respectively. The main peak of C–S–H is coincident with the main peak of calcite 30.3 nm (29.5°), but the halos between 25° and 40° are characteristic of C–S–H phase.

CRI deteriorated layer presented only two crystalline mineral species clearly identified: calcite and chrysotile. Peaks of high Ca/Si C–S–H [18] do not appear in the deteriorated layer. The C–S–H halo is less intense than the halos of other samples (see detail in Fig. 3). This relates to a decrease in the amount of C–S–H during the deterioration process. Calcium sulfate dehydrate was not detected in CRI samples. The presence of calcium sulfate dehydrate is associated to ettringite carbonation reaction as demonstrated in Eq. (3). In addition to the mentioned minerals, Portlandite was identified in the CRI-core samples, but not in the deteriorated layer. Perhaps gypsum from the sulfate attack of the outer layer dissolved by rainwater and infiltrated into the core.

Figs. 4 and 5 present TG and DTG curves respectively. Fig. 6 consolidates the weight losses from the TG tests, expressed as a percentage of total fractions. The main compounds that decompose thermally up to 350 °C (1st peak)

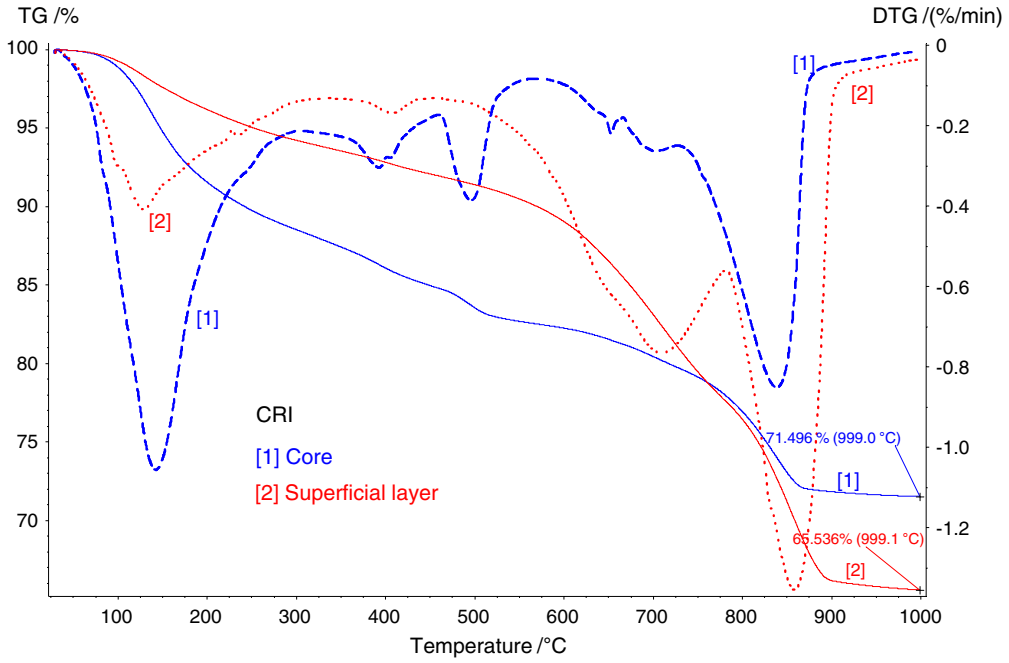

Fig. 5. TG and DTG curves of samples extracted from the deteriorated layer and the core region of CRI specimens.

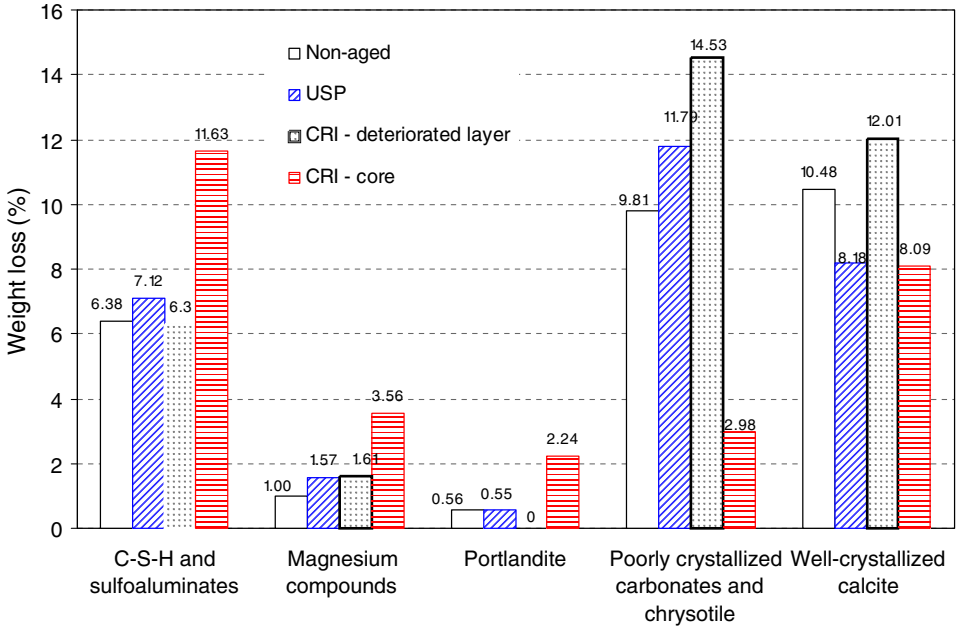

Fig. 6. Loss of weight on TG analyses.

are C–S–H, ettringite and gypsum [3,19]. From about 350 to 450 °C (2nd peak), thermal decomposition of magnesium compounds and chrysotile fiber takes place, although of little contribution. Thermal decomposition of Portlandite ($Ca(OH)_2$) occurs around 450 °C (3rd peak), followed by poorly crystallized calcite [17], dolomite and chrysotile fibers in the range between 500 and 800 °C [20] and by well-crystallized calcite at temperatures above 800 °C [15,18]. TG and DTG curves of non-aged and USP samples are similar. The discreet peak on shoulder that appears in the DTG curve of non-aged sample at about 780 °C (Fig. 4) indicates thermal decomposition of the dolomite fraction from calcareous filler.

The TG results of CRI samples corroborate to the existence of two layers. The CRI-deteriorated layer has no weight loss related to Portlandite decomposition. This implies that the available C–S–H has a 1.7 Ca/Si ratio or less [18], which is consistent with XRD results. Weight loss of the deteriorated layer up to 350 °C is 6.3%, a value much lower than core (11.63%). Therefore, the total amount of C–S–H and sulfate compounds (ettringite, gypsite and sulfoaluminates) is also lower than in the core. On the other hand, the amount of carbonates plus asbestos in the deteriorated layer is more than two times higher than the content of the core, since the TG weight loss from 500 up to 1000 °C is 26.5% in the deteriorated layer, against 11.1% in the outer layer.

The data presented in Table 2 show that there is little difference in the chemical composition of non-aged samples, USP and CRI-core. Table 3 presents the insoluble residue content of each sample. Asbestos and cellulose fibers, the insoluble fraction of cement and calcareous filler, are the main phases of the insoluble residue of asbestos-cement based material. The content of insoluble residue in the deteriorated layer is 100% higher than in the core of CRI samples, confirming the occurrence of leaching in the outer layer. It also confirms, the amount of matrix leached is proportionally twice higher than the amount of fibers eventually liberated into the environment. Surprisingly, this leaching had no other significant impact on the chemical composition of the outer layer, which remained quite similar to that of the core (Table 2), despite the important changes in mineral composition.

Considering that insoluble residues are only composed of chrysotile fibers, and considering the contribution of chrysotile fiber weight loss (~13% of chrysotile fiber content) at temperature ranges of 500–1000 °C, it is possible

Table 2
Chemical composition by X-rays fluorescence: % of oxides referred to the ignited mass, normalized to 100%

Measured item	Non-aged	USP	CRI-core	CRI-deteriorated layer
MgO	7.07	7.09	6.34	5.97
Al_2O_3	2.55	3.13	3.09	3.00
SiO_2	15.60	6.50	17.00	16.20
SO_3	2.21	2.17	2.65	1.36
CaO	65.50	63.80	64.60	65.50
Fe_2O_3	5.52	5.63	4.68	5.48
Others	1.60	1.70	1.70	2.47
Total	100.05	100.02	100.06	99.98

Table 3
Loss on ignition (LOI) and insoluble residue

Measured item	Non-aged	USP	CRI-core	CRI-deteriorated layer
LOI obtained in TG tests (% of total weight)	28.24	29.21	28.50	34.46
Insoluble residue (%) (wet analysis)	16.6	20.0	11.3	22.7

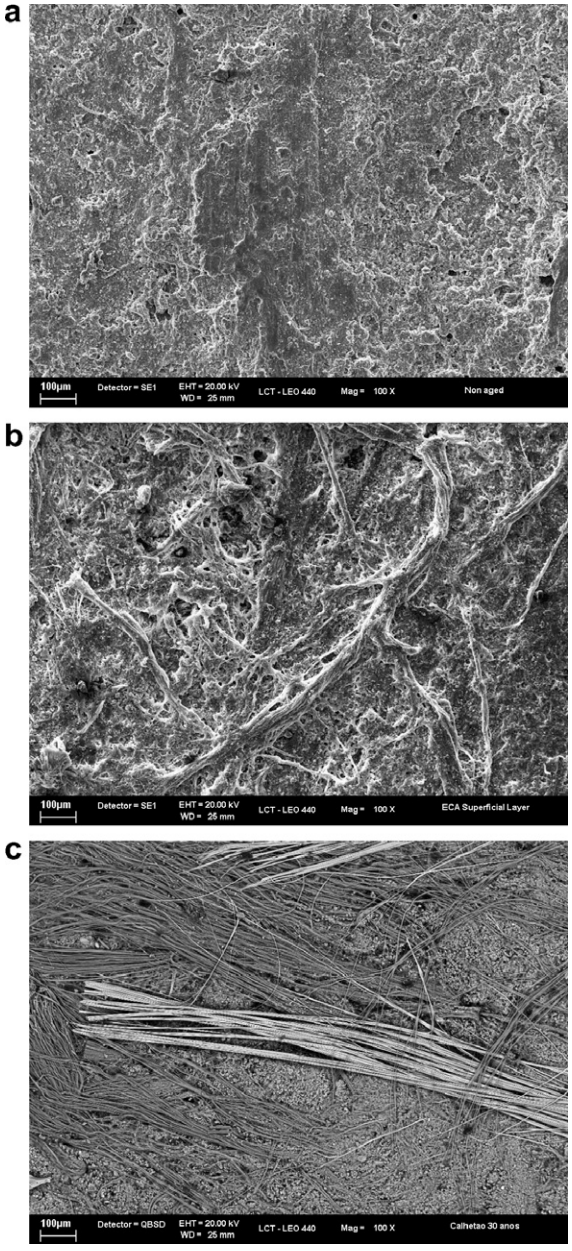

Fig. 7. Superficial layers: (a) secondary electron image of non-aged sample, (b) secondary electron image of USP sample and (c) backscattering electron image of CRI sample.

to estimate the amount of carbonate compounds in all samples. Non-aged and USP samples presented approximately 40% of carbonates while CRI-core presented 22% and CRI-deteriorated layer, 54%.

3.3. SEM and porosity evaluation

Fig. 7 shows the differences between the outer surfaces of non-aged and aged samples (USP and CRI). No fibers were identified on the surfaces of the non-aged samples. A patina covered the surface of the USP sample that was exposed to the weather during its service life. Removing the patina revealed that surface leaching had partially exposed the fibers despite still being covered by some cement paste. However, at the top surface of the CRI roof sheet, clean fiber strands were clearly visible after washing, confirming a strong leaching process (Fig. 7). Visual analysis of CRI sample surfaces detected the presence of a low amount of blue fibers, probably crocidolite fibers (blue asbestos). Fig. 8 shows a backscattering image of the two types of asbestos fibers (crocidolite and chrysotile) on the surface of the CRI sample. Fe and Na elements were detected in the composition of one of these fibers, confirming that they are crocidolite (Fig. 8a). The most expressive event in the thermal decomposition of crocidolite fibers occurs at about 700 °C. However, there is little contribution to weight loss of the composite in this range (~3 wt.% of crocidolite content).

Asbestos fiber strands were observed in the fractured section of USP (Fig. 9) and CRI specimens (Fig. 10a and b). Hydration products did not fill in the inter-fiber space in strands despite being exposed to water for a long time.

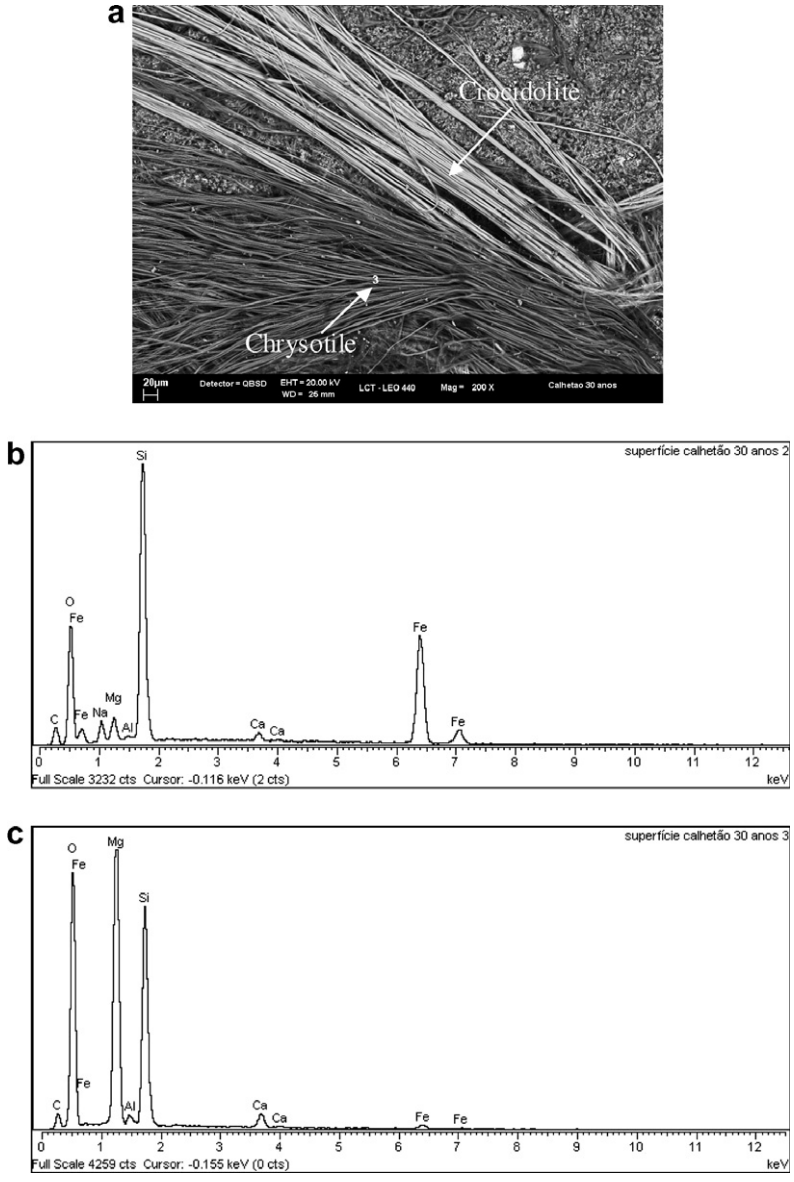

Fig. 8. Superficial layer of a CRI specimen: (a) backscattering electron image of two different types of asbestos fibers; (b) EDS of crocidolite fibers and (c) EDS of chrysotile fiber.

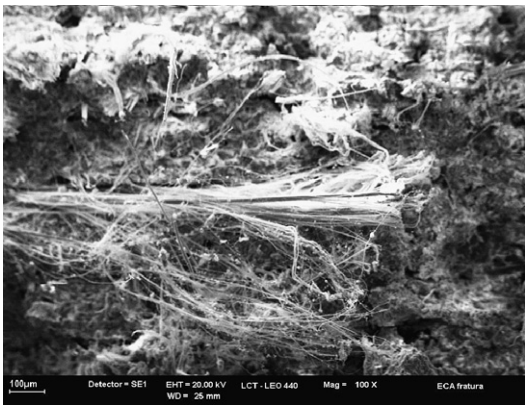

Fig. 9. Secondary electron image of fracture section of USP specimen: detail of asbestos fibers cluster.

Consequently, fibers may be liberated during the fracture and leaching processes of the asbestos-cement. These fibers do not show any signs of deterioration (Fig. 9). This confirms the conclusions of Studinka [21] and Bentur and Mindess [1] concerning the chemical compatibility between asbestos fibers and cement matrix.

Cellulose fibers were easily identified in the non-aged samples. CRI samples revealed none and USP very few fibers and these were completely petrified (Fig. 11). Bentur and Akers [22] have reported this mechanism of deterioration in an earlier study. Petrified cellulose fibers looked darker in the BSE due to the lower atomic number of carbon (Fig. 11b) and presented a higher amount of carbon (Fig. 11d) when compared to the matrix (Fig. 11c) in the EDS analysis.

USP and non-aged samples present lower porosities (average of ~26% for both) than CRI samples (average ~39% for both core and deteriorated layer). Fig. 12 presents the pore size and distribution curve. The peak below 10 nm is related to the cement paste and the peaks between 100 nm and 1000 nm are capillary pores resulting from the manufacturing process. The number of voids inside the asbestos strands and cellulose fibers in fiber cement actively influences the peak between 100 nm and 1000 nm. The higher porosity of the CRI-core layer is probably due to the core not being yet carbonated and of the voids in fiber strands (Fig. 10a). CRI-deteriorated layer revealed a coarsening of pores greater than 200 nm in comparison with the core layer. Coarsening has been associated to the SiO_2 (gel) formation during carbonation of C–S–H [23] and leaching of the cement matrix [24].

3.4. Mechanical performance

Fig. 13 presents typical curves of flexural stress versus specific deflection. Table 4 presents MOR, MOE and toughness results. Despite the absence of information concerning the raw materials and formulations used in the pro-

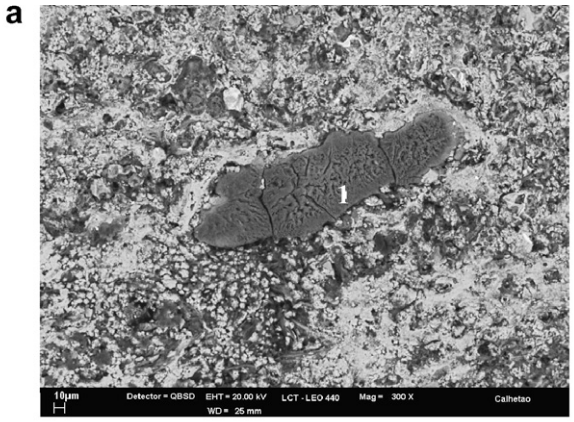

Fig. 10. CRI-core sample: (a) backscattering electron image of polished section and (b) EDS line-scan of point 1 (asbestos fibers).

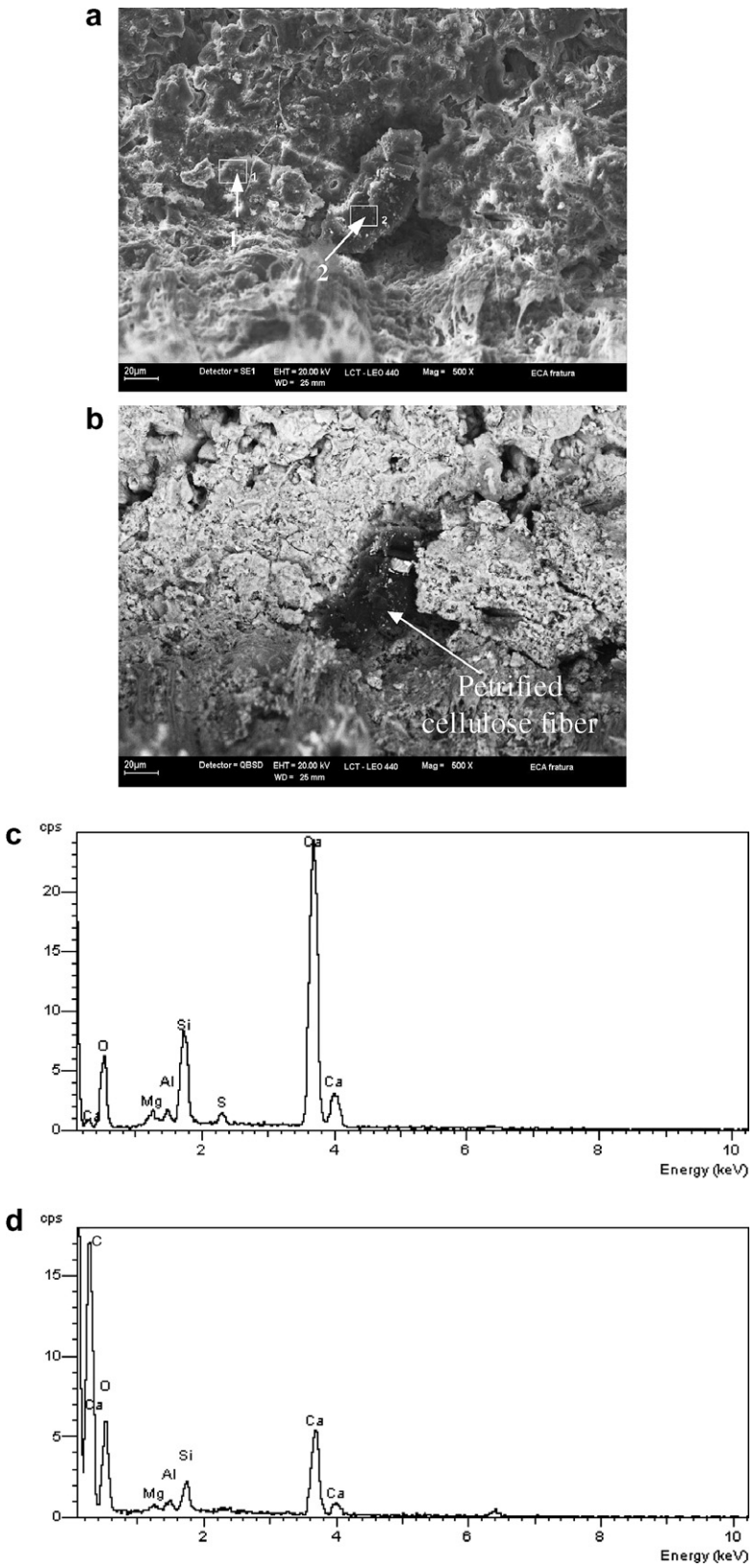

Fig. 11. Fracture section of USP specimen: (a) secondary electron image showing the matrix (region 1) and a petrified cellulose fiber (region 2); (b) backscattering electron image showing the petrified cellulose fiber; (c) EDS of matrix (region 1) and (d) EDS of cellulose petrified fiber (region 2).

duction of the fiber-cement under evaluation in this study, a comparative analysis is still possible. The USP samples, which had been in service for 37 years, presented mechanical behavior similar to that of the non-aged samples at

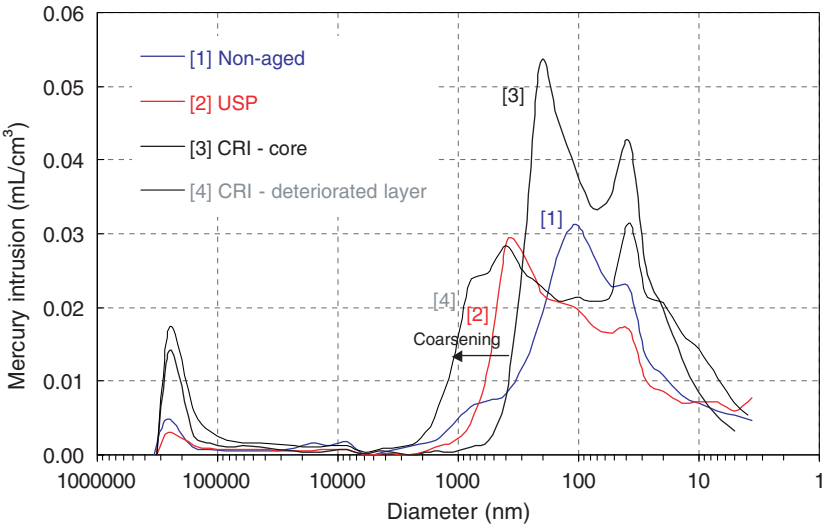

Fig. 12. Pore size distribution of samples.

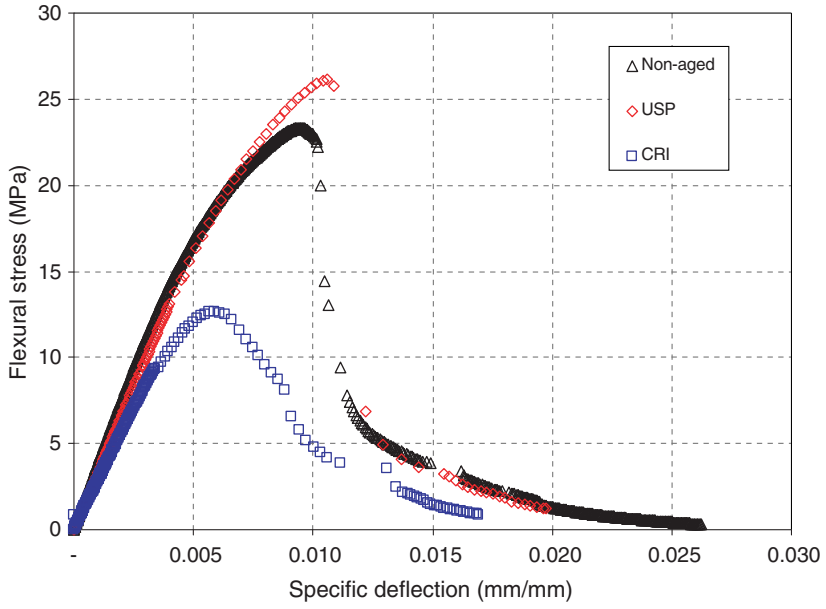

Fig. 13. Typical curves of flexural stress versus specific deflection (deflection/span) of specimens.

Table 4
Mechanical properties

Samples	Modulus of rupture (MOR) (MPa)	Modulus of elasticity (MOE) (GPa)	Toughness (kJ/m^2)
Non-aged	23.9 ± 2.3	19.4 ± 1.3	1.21 ± 0.25
USP	24.9 ± 2.5	18.9 ± 1.8	1.06 ± 0.35
CRI	13.5 ± 1.0	11.3 ± 0.7	0.93 ± 0.04

significance level of 0.05. On the other hand, CRI specimens presented lower values of MOR and MOE due to the higher porosity and the lower strength of the deteriorated superficial layer. Except from matrix deterioration due to environmental factors, asbestos cement does not appear to suffer significant mechanical deterioration, even after almost 40 years. This is in agreement with remarks from Bentur and Mindess [1].

The most plausible explanation for the mechanism of matrix deterioration of CRI samples is as follows: (a) production of ettringite due to sulfate attack consuming the Portlandite and reducing Ca/Si from C–S–H; (b) decomposition of ettringite by carbonation according to Eq. (3) producing $CaCO_3$,detected in both TG and XRD, and $CaSO_4 \cdot 2H_2O$; (c) $CaSO_4 \cdot 2H_2O$ is leached out by rain water, leaving low C/S C–S–H, $CaCO_3$, amorphous material and an insoluble fraction which includes fibers. As a result, the leached surface has a higher content of insoluble phase and lower content of SO_3. Consequently, the mechanical properties of the CRI composite are lower than

the other samples under evaluation. Carbonation was the only relevant aging transformation for the USP sample, which affected the whole component.

4. Conclusions

Aging affects the properties of asbestos-cement corrugated sheets, which are directly influenced by the environment to which they are exposed. The 37 year-old asbestos-cement from the city of São Paulo presented mechanical performance similar to the non-aged asbestos-cement commercially available in the Brazilian market. Carbonation of the matrix was the main alteration of the asbestos-cement corrugated sheets from São Paulo. In contrast, the 30 year-old asbestos-cement from the Criciúma, which has been exposed to intense acid rain, showed deterioration compatible with sulfate attack, carbonation and leaching. Pore size distribution of the superficial layer and core, mineralogical composition and mechanical performance are undeniable indications of these effects. The MOR of these samples was also lower than that of the other samples from USP São Paulo and non-aged sheets.

As a consequence, we conclude that surface leaching can have significant mechanical impact in the thin sheets of fiber-cement, potentially limiting the component service-life. So interpretation of the results of natural or accelerated aging tests should always consider the climatic and other environmental conditions.

Very little surface leaching was observed in the samples exposed in São Paulo, with some fiber strands being only partially exposed after 37 years. However, outer surface analysis of the roof sheets from the more aggressive, acid rain environment of Criciúma showed many visible, partially bonded long strands of clean fibers. Nevertheless the amount of leached matrix is proportionally higher than the amount of fiber eventually liberated into the environment.

Acknowledgement

The authors would like to thank the Fundação de Amparo à Pesquisa do Estado de São Paulo (FAPESP), CNPq, Financiadora de Estudos e Projetos (FINEP, HABITARE Program), INFIBRA and IMBRALIT for their financial support.

References

[1] Bentur A, Mindess S. Fibre reinforced cementitious composites. London and New York: Elsevier Applied Science; 1990.
[2] Gram H-E. Natural fibre concrete roofing, Concrete technology and design 5: natural fibre reinforced cement and concrete, Glasgow and London; 1988.
[3] Taylor HFW, editor. Cement chemistry. Thomas Telford; 1997.
[4] Faucon P, Le Bescop P, Adenot F, Bonville P, Jacquinot JF, Pineau F, et al. Leaching of cement: study of the surface layer. Cement Concrete Res 1996;26(11):1707–15.
[5] Carde C, François R. Modeling the loss of strength and porosity increase due to the leaching of cement pastes. Cement Concrete Comp 1999;21:181–8.
[6] Babic BR. The use of cement fibre composites in prolonged wet environments. In: 10th international inorganic-bonded fiber composites conference, 2006. p. 260–73.
[7] Gollop RS, Taylor HFW. Microstructural and microanalytical studies of sulfate attack – I ordinary Portland cement paste. Cement Concrete Res 1992;22:1027–38.
[8] Sabbione C, Bonazza A, Zappia G. Damage on hydraulic mortars: the Venice Arsenal. J Cult Heritage 2002;3:83–8.
[9] Beddoe RE, Dorner HW. Modeling acid attack on concrete: Part I. The essential mechanisms. Cement Concrete Res 2005;35:2333–9.
[10] Xie S, Qi L, Zhou D. Investigation of the effects of acid rain on the deterioration of cement concrete using accelerated tests established in laboratory. Atmos Environ 2004;38:4457–66.
[11] Zivica V, Bajza A. Acidic attack of cement based materials – a review: Part 1. Principle of acidic attack. Constr Build Mater 2001;15(8):331–40.
[12] Manns W, Wesche K. Variation in strength of mortars made of different cements due to carbonation. In: Proceedings of the international symposium on the chemistry of cement, Part III II/4, 1969. p. 385–93.
[13] John VM, Cincotto MA, Sjöström C, Agopyan V, Oliveira CTA. Durability of slag mortar reinforced with coconut fibre. Cement Concrete Comp 2005;27:565–74.
[14] Chen XT, Zou RZ, Chen XR. Kinetic-Study of ettringite carbonation reaction. Cement Concrete Res 1994;24(7):1383–9.
[15] Sato NMN. Porosity and mass transport on concrete [Thesis of Polytechnic School of University of São Paulo], São Paulo, 1998 [In Portuguese].
[16] Barr B, Gettu R, Al-Oraimi SKA, Bryana LS. Toughness measurement – the need to think again. Cement Concrete Comp 1996;18:281–97.
[17] Cole WF, Kroone B. Carbon dioxide in hydrated Portland cement. J Am Concrete Inst 1960;31:1275–95.
[18] Chen JJ, Thomas JJ, Taylor HFW, Jennings HM. Solubility and structure of calcium silicate hydrate. Cement Concrete Res 2004;34(9):1499–519.
[19] Ramachandran VS. Applications of differential thermal analysis in cement chemical. New York: Chemical Publishing Company; 1969.
[20] Gualtieri AF, Tartaglia A. Thermal decomposition of asbestos and recycling in traditional ceramics. J Eur Ceram Soc 2000;20:1409–18.
[21] Studinka JB. Asbestos substitution in the fibre cement industry. Int J Cement Compos Lightweight Concrete 1989;11:73–8.
[22] Bentur A, Akers AS. The microstructure and ageing of cellulose fibre reinforced cement composites cured in a normal environment. Int J Cement Compos Lightweight Concrete 1989;11(2).
[23] Bier ThA, Kropp J, Hilsdorf HK. Carbonation and realkalinization of concrete and hydrated cement paste. In: Durability of construction materials 3, Proceedings of the 1st congress from materials science to construction materials engineering, RILEM, 1987.
[24] Haga K, Sutou S, Hironaga M, Tanaka S, Nagasaki S. Effects of porosity on leaching of Ca from hardened ordinary Portland cement paste. Cement Concrete Res 2005;35(9):1764–75.